

EVALUATION OF STALL BEHAVIOUR OF T-TAIL AIRCRAFT: MODELLING AND FLIGHT TEST

Mark Lowenberg[1] & Daniel Pusztai[1]

[1]School of Civil, Aerospace & Design Engineering, University of Bristol, UK

Abstract

A new stall model aimed at investigating aircraft flight dynamics under impending stalls, and post-stall conditions is presented. It is designed to capture the characteristic behaviour of swept-wing transport aircraft with a T-Tail empennage: an unstable pitch break and wing rock during an approach to stall. This study builds on previous work based on the NASA GTT (Generic T-Tail) aircraft geometry and leverages wind tunnel and sub-scale flight test data for the model identification. Results are shown in the form of time history simulations and bifurcation diagrams against real-word stall data from flight test. The proposed model shows a good improvement from the baseline wind tunnel models in predicting pitch-up and onset of wing rock during an approach to stall. The incorporation of bifurcation analysis into the suite of tools used to assess nonlinear behaviours, combined with a new approach to the modeling of asymmetric wing stall, fills an important gap in predicting lateral-directional instabilities at stall where other techniques so far failed to yield accurate predictions.

Keywords: flight dynamics; stall model; model flight test; wing rock; bifurcation analysis.

1. Introduction

The creation of mathematical models of aerodynamic forces and moments in regions of the flight envelope where nonlinear flow phenomena are significant is challenging. Whilst transport aircraft normally do not operate under such conditions, the investigation of upset and loss-of-control (LOC) incidents and accidents does require conducting such studies beyond the intended operating envelope. An upset, which is defined as extreme aircraft attitudes in combination with airspeeds that are unsuitable to sustain flight, usually involves separated flows and may lead to asymmetric wing stall and incipient spin. Determining a mathematical model to adequately represent the aerodynamic loads in the approach to stall and the transient responses post-stall is difficult both computationally and experimentally, and full-scale flight tests are not usually feasible due to the inherent risk of a LOC.

This paper extends previous studies of the NASA Generic T-Tail (GTT) airliner configuration with a focus on deep stall and subsequent spin entry. The earlier work entailed a series of wind tunnel and water tunnel tests conducted over a wide incidence and sideslip envelope, accompanied by CFD analysis, by NASA [1,2] from which the “NASA GTT” aerodynamic model was developed (for the wind-tunnel-scale model and for higher Reynold number corresponding to full-scale flight conditions facilitated by the CFD) and evaluated in simulations [3]. This was followed by work at the University of Bristol (UoB) in which a copy of the NASA wind tunnel model was tested statically in the UoB 7′x5′ tunnel over the same envelope as in NASA’s tests [4], and two remote-controlled free-flying models were built and flight tested [5] (Figure 1). The flights tests covered normal flight conditions through to deep stall and attempted recovery. These studies culminated in a wide-envelope numerical model based on wind tunnel experiments, as well as a nonlinear mathematical model identified from flight tests [6]. Finally, a comparison of a deep stall flight test trace was made with bifurcation diagrams computed from both the NASA model and the UoB wind tunnel data [7]: such diagrams provide the ‘structure’ of the steady state dynamics underlying the behaviour of the system and supplement more

https://doi.org/10.71945/icas2026_0518

traditional ways of comparing the numerical model with the physical model responses.

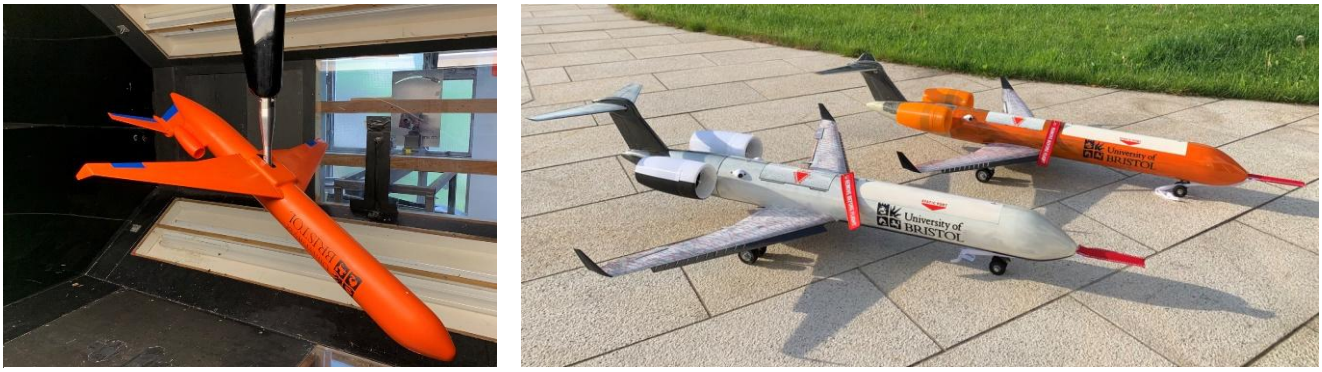


Figure 1: UoB GTT wind tunnel (left) and free-flight (right) models.

In this paper, these previous studies are extended through the development of an improved stall model intended to capture the lateral-directional motions that arise in the stall region and a closer match with experiments of the transition to stall and deep stall. The model is an extension of the stall model in [6] and is designed to retain a simple structure to allow for efficient computations including numerical continuation to generate bifurcation diagrams.

The wind tunnel and free flight models are first described briefly in Section 2, followed by a summary of the nature of the separated flow development in flight tests, and associated aircraft responses, in Section 3. The new stall model is explained in Section 4 and the evaluation thereof presented in Section 5, prior to conclusions and recommendations for further work in Section 6.

2. GTT wind tunnel and free flight models

NASA defined its Generic T-Tailed (GTT) transport model in order to study upset/LOC of such configurations. A mathematical model of the aerodynamics was generated from data produced in experiments in the Langley Research Center 12′ Low-Speed Tunnel, the Boeing Flow Visualisation Water Tunnel and Boeing North American Aviation Research Tunnel; these were supplemented by CFD studies to resolve results from the different tunnels and generate corrections for full-scale Reynolds number [1]. The aerodynamic data covers the incidence and sideslip range $-8° \le \alpha \le +60°$ and $-35° \le \beta \le +35°$ respectively, to facilitate upset studies.

At UoB, this aerodynamic model – provided by NASA Langley – was incorporated within the standard 6-degree-of-freedom nonlinear equations of motion to create a flight dynamics model that could be used for time history simulations, bifurcation analysis, control law design and evaluation, etc. In addition, a 3.7% scale wind tunnel that is an exact replica of the one tested in the Langley 12′ tunnel was built by the second author at the University of Bristol. This was tested over a wide α and β envelope in the UoB 7′x5′ low-speed tunnel using the ATE Aerotech six-component overhead balance[1].

Two radio-controlled free-flight models with actuated control surfaces were also designed and constructed, to the same scale and geometry apart from the following modifications required to facilitate flight tests: a fixed tricycle landing gear, leading edge Krueger flaps and trailing edge single-slotted flaps, and 50% larger engine nacelles (to accommodate the ducted fans). The scaled characteristic dimensions of the flying models are shown in **Error! Reference source not found.**. Note that the all-moving stabiliser was used for pitch control in flights tests rather than the elevator since wind tunnel results indicated a similar control effectiveness.

A second version of the wind tunnel model was built to incorporate the changes of the free-flight model relative to the original in order to assess the impact of the model changes – and which were found to be minor [4]. Furthermore, they are not considered a limitation in the current work since the focus is on

[1] Dynamics tests, including in multiple degrees of freedom, are still to be carried out on this model. NASA's values of damping derivatives are used in the mathematical model.

evaluating mathematical models against flight test data, and the wind tunnel data used to generate the nonlinear maths model was based on the free-flight geometry. Tufts were used on both the wind tunnel and the flying models (the latter observed through two wide-angle cameras on the rear fuselage) to provide surface flow visualisation.

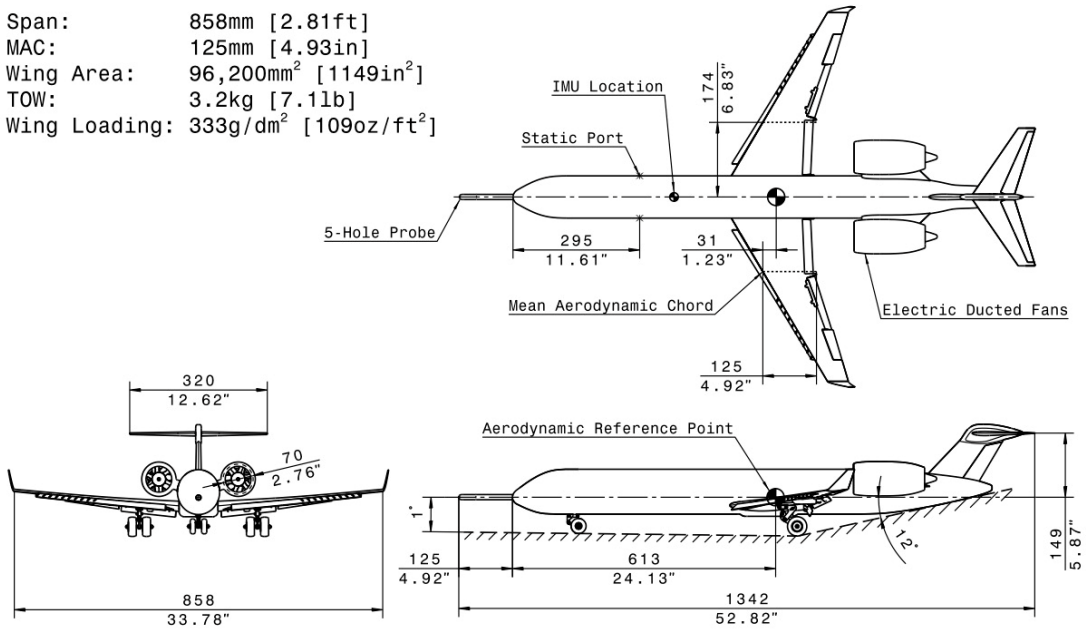


Figure 2: Geometry of UoB GTT models with dimensions in mm (in).

3. Stall model

As a result of the previous wind tunnel campaigns and CFD studies, numerical models of the GTT's aerodynamics were already developed by NASA and the UoB. One of the primary goals of the GTT's sub-scale flight test campaign was to investigate the accuracy of these models, especially when flying near or at stall. The experiments showed good agreement to theoretical predictions but some shortcomings were pointed out [5–7]. In particular, it was observed that the flight test aircraft exhibited a later-than-anticipated pitch break, as well as a more severe wing rock during an approach to stall. Although the basic principles behind these effects are generally well understood, little research has been conducted to model these effects. To better highlight the requirements a suitable stall model needs to fulfil, the GTT's stall behaviour is briefly described in the following paragraph (refer to [6] for a more in-depth discussion).

As typical for all modern transport aircraft, the GTT features a swept-back wing to reduce wave drag at transonic cruise speeds, but such wings usually suffer from poor low-speed performance due to the risk of tip stalls: the outboard wing sections experience earlier flow separation than the wing roots. This is caused by the large spanwise flows on swept wings, which in turn increase the local upwash and reduce the critical angle of attack (AoA) at the wing tips. Figure 2 shows the progression of flow separation on the GTT's wing through tuft pictures obtained during the UoB wind tunnel tests [4]. It is observed that tip stall starts at a free-stream AoA as low as 5°, causing a redistribution of lift along the wing span and a forward shift of the centre of pressure. This creates a destabilising nose-up pitching moment and effectively forces the minimum safe flying speed to be faster than the actual stall speed[2]. Figure 2 shows stall patterns under symmetric conditions, but this is rarely achievable in reality. Any small stall asymmetry will create a net rolling moment towards the wing with greater separated flow. This wing is now experiencing an additional plunge velocity, increasing the local AoA even further. Additionally, stalled sections operate at a negative lift gradient, which also contributes to an overall

[2] Defined here as the lowest possible speed under which 1-g level flight can be achieved. This speed relates to the first peak in the lift coefficient.

reduction in roll damping moments and further exacerbates the roll instability. Both effects drive the roll-off behaviour during stall that can eventually turn into wing rock if uncorrected. Figure 3 depicts the asymmetrically separated flow during a flight test where wing rock was encountered.

In [6] it was shown that the GTT's wing rock mode of oscillation is a pure body-axis roll, which creates kinematic coupling between AoA and sideslip as bank angle varies. This is visualised in Figure 4, which shows the momentary wing separation at peak amplitude during a wing rock cycle: AoA is reduced below the critical point and flow is mostly re-attached on both wings. At the same time sideslip is large, creating a restoring rolling moment due to the typically large static lateral stability coefficient C_{l_β} for swept wings. Wing rock is therefore an exchange between the destabilising rolling moments due to asymmetric stall and the large stabilising dihedral effect of a swept wing, aided by the restoration of lift on the downgoing wing due to kinematic coupling.

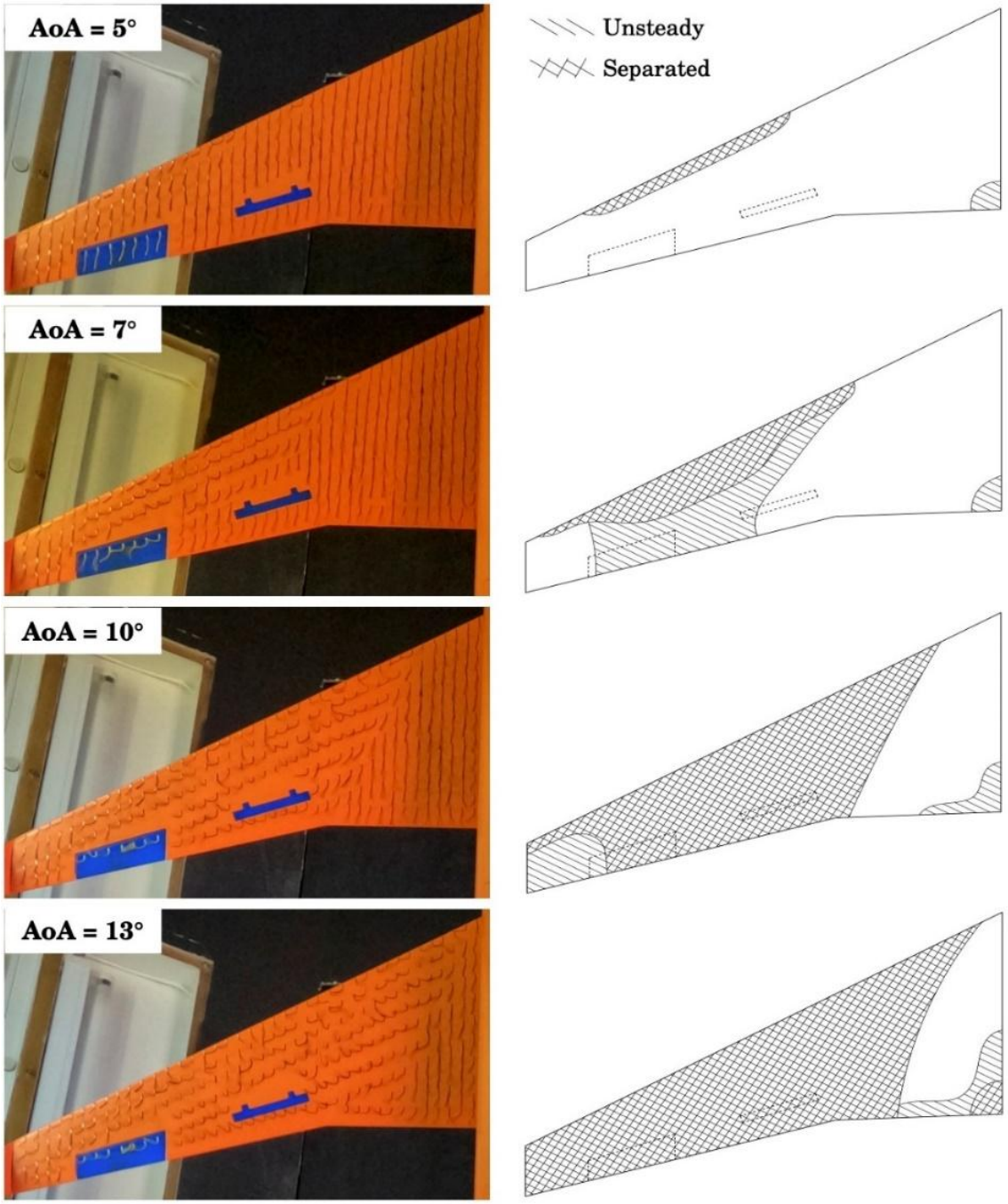


Figure 2: Stall progression on the GTT's main wing (clean configuration).

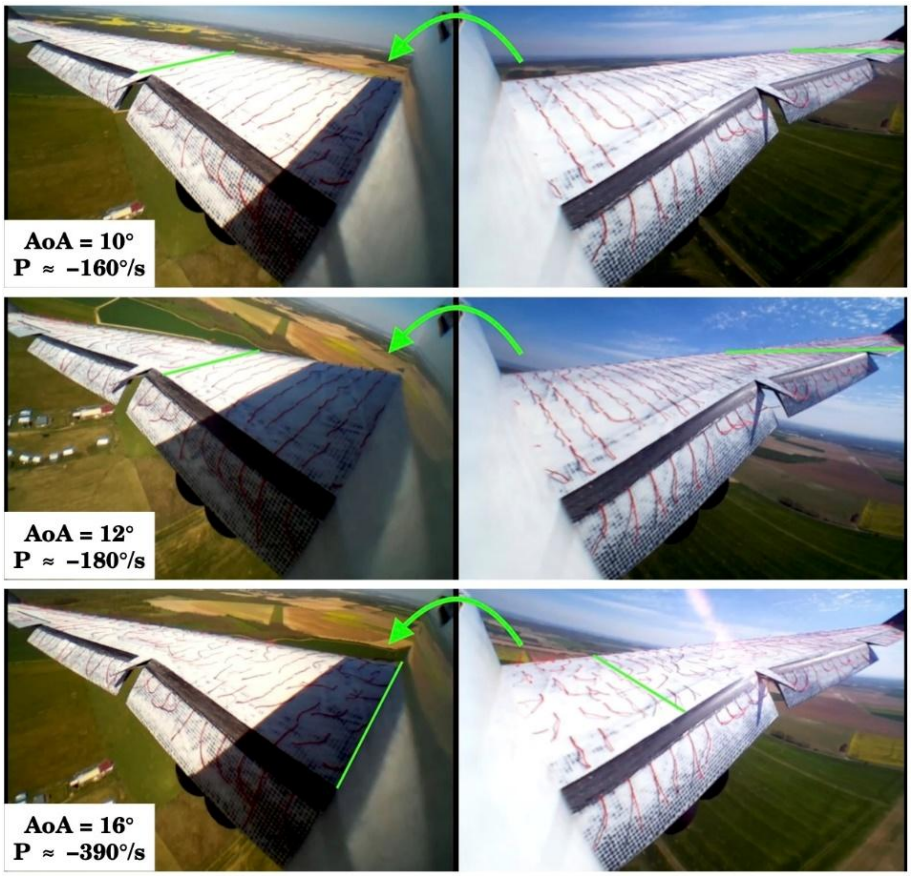


Figure 3: Flow separation on the GTT's main wing during wing rock.

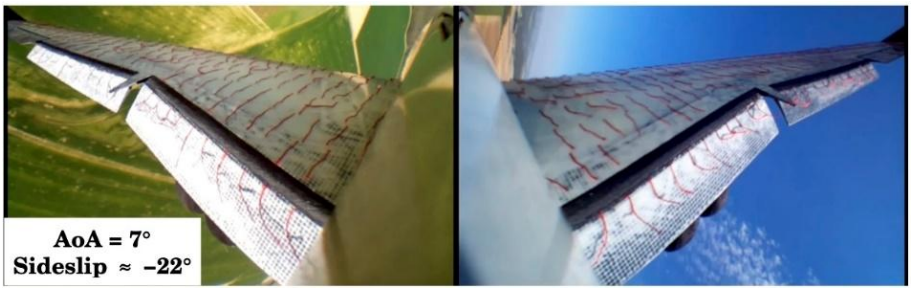


Figure 4: Flow re-attachment at peak wing rock amplitudes.

The stall model presented in this work uses a basic linear aerodynamic representation as a starting point (Eq. (1)-(6)), with the free parameters previously being identified during the GTT flight test campaign [6]. Such a model is usually easily obtainable for any aircraft and is sufficient to capture basic aircraft dynamics under normal flight conditions.

$$C_L = C_{L0} + C_{L\alpha}\,\alpha + C_{L\hat{Q}}\,\hat{Q} + C_{L\delta_S}\,\delta_{stab} \tag{1}$$

$$C_m = C_{m0} + C_{m\alpha}\,\alpha + C_{m\hat{Q}}\,\hat{Q} + C_{m\delta_S}\,\delta_{stab} \tag{2}$$

$$C_D = C_{D0} + \frac{C_L^2}{\pi\, e\, AR} \tag{3}$$

$$C_S = C_{S\beta}\,\beta + C_{S\hat{P}}\,\hat{P} + C_{S\hat{R}}\,\hat{R} + C_{S\delta_R}\,\delta_{rud} \tag{4}$$

$$C_l = C_{l\beta}\,\beta + C_{l\hat{P}}\,\hat{P} + C_{l\hat{R}}\,\hat{R} + C_{l\delta_A}\left(\delta_{ail,left} + \delta_{ail,right}\right) + C_{l\delta_R}\,\delta_{rud} \tag{5}$$

$$C_n = C_{n\beta}\,\beta + C_{n\hat{P}}\,\hat{P} + C_{n\hat{R}}\,\hat{R} + C_{n\delta_A}\left(\delta_{ail,left} + \delta_{ail,right}\right) + C_{n\delta_R}\,\delta_{rud} \tag{6}$$

The notation in these equations follows standard flight dynamics notation, with $\hat{P}$, $\hat{Q}$ and $\hat{R}$ being non-

dimensionalised roll, pitch and yaw rates respectively; δ_{stab}, δ_{ail} and δ_{rud} are stabiliser, aileron and rudder deflections normalised by their maximum respective deflection ranges.

The progression of flow separation on any arbitrary wing section is now defined as follows:

$$X_C = 0.5\left[1 - \tanh\left(s\left(\alpha_C - \alpha^*\right)\right)\right] \tag{7}$$

This equation is adopted from [9,10] and often used to model stall effects of whole lifting surfaces. The flow separation state X_C, varying between 1 for fully attached and 0 for fully separated flow, is calculated from the local AoA α_C, the critical AoA of the aerofoil section α^*, and the shape parameter s, defining the stall abruptness. The formulation presented here slightly differs from the classic one in two respects:

1. Time dependencies are dropped[3] since wind tunnel results do not justify including them. Although this aligns well with other flight test research on aircraft stall [11], such effects cannot be ruled out with full certainty. Nevertheless, it will be later shown that good results are achieved with the proposed quasi-steady model.
2. Separation is assumed to start from the leading edge. Although this would be very uncommon for an isolated aerofoil, we have to consider each section as part of the complete swept wing, where the influence of large spanwise flows causes a leading edge stall.

In order to define the local stall progression according to (Eq. (7)), the free parameters α^* and s, and the local flow AoA α_C must be determined. The former two are assumed to be constant since they depend on the aerofoil shape, which remains approximately the same across the GTT's wing span. The local AoA on the other hand is split into four components (Eq. (8)): the free-stream AoA α_0, the geometric section twist $\Delta\alpha_{\mathrm{geo}}$, the induced upwash due to wing sweep $\Delta\alpha_{\mathrm{sweep}}$, and the upwash due to roll rate $\Delta\alpha_{\mathrm{roll}}$.

$$\alpha_C = \alpha_0 + \Delta\alpha_{\mathrm{geo}} + \Delta\alpha_{\mathrm{sweep}} + \Delta\alpha_{\mathrm{roll}} \tag{8}$$

With exception of the free-stream AoA, each component is a function of wing span. The geometric wing twist, or washout, is known for a given airframe and is usually designed into the wing to counteract the induced upwash due to wing sweep, which in turn is assumed to vary linearly with wingspan:

$$\Delta\alpha_{\mathrm{sweep}} = \Delta\alpha_{\mathrm{tip}} \frac{|y| - y_{\mathrm{root}}}{y_{\mathrm{tip}} - y_{\mathrm{root}}} \tag{9}$$

Finally, the change in local AoA due to roll rate is a simple geometric relation based on the local flow vectors:

$$\Delta\alpha_{\mathrm{roll}} = \arctan\left(\frac{\mathrm{P}\, y}{V_T}\right) = \arctan\left(\frac{\bar{\mathrm{P}}\, y}{b/2}\right) \tag{10}$$

With the local flow state (Eq. (7)) defined for every spanwise aerofoil section, a separation boundary can be drawn onto the wing planform, similarly to what is shown in Figure 2. The global separation parameter X_W is then defined as the relative area of the wing that is not yet stalled:

$$X_W = \frac{\int_{y_{\mathrm{root}}}^{y_{\mathrm{tip}}} c\, X_C \,\mathrm{d}y}{\int_{y_{\mathrm{root}}}^{y_{\mathrm{tip}}} c \,\mathrm{d}y} \tag{11}$$

Equations (8)-(11) reduce to three unknowns: the section critical AoA α^*, the stall abruptness s, and the upwash at the wing tip $\Delta\alpha_{\mathrm{tip}}$. These parameters have to be appropriately chosen to match the stall progression at every AoA from onset of wing stall up to full flow separation. This was achieved by processing tuft images with MATLAB's Image Processing Toolbox and solving an optimisation problem for the model parameters, yielding:

[3] This effectively eliminates the usual differential equation associated with the flow separation states. As such, they will be referred to as "parameters" for the reminder of the report as they carry no time-dependency anymore.

- $\alpha^* = 15.3°$
- $s = 18.9$
- $\Delta\alpha_{\text{tip}} = 10.6°$

No 2D aerodynamic data is available for the GTT's transonic aerofoil, therefore a direct comparison for the section critical AoA α^* and the stall abruptness s is not possible, although both values are within a reasonable range of what can be expected from wind tunnel experiments on the full aircraft [6]. The induced upwash at the wing tip may seem high at a first glance but is also matching expectations considering that tip separation is observed at a global AoA as low as 6°. Figure 5 shows the result of evaluating the global separation parameter (Eq. (11)) compared to a simple stall model previously obtained from flight test ("Flight test ID" in [6]). Due to the technique outlined above, the new stall model matches the actual flow separation progression much closer. Additionally, Figure 6 depicts a plan view of the left and right wing with the predicted separation lines indicated. This figure also shows the effect of a non-zero roll rate as is experienced during the wing rock, causing asymmetric stall patterns. This feature is essential to accurately capturing the wing rock dynamics, which will be evaluated later in the results section.

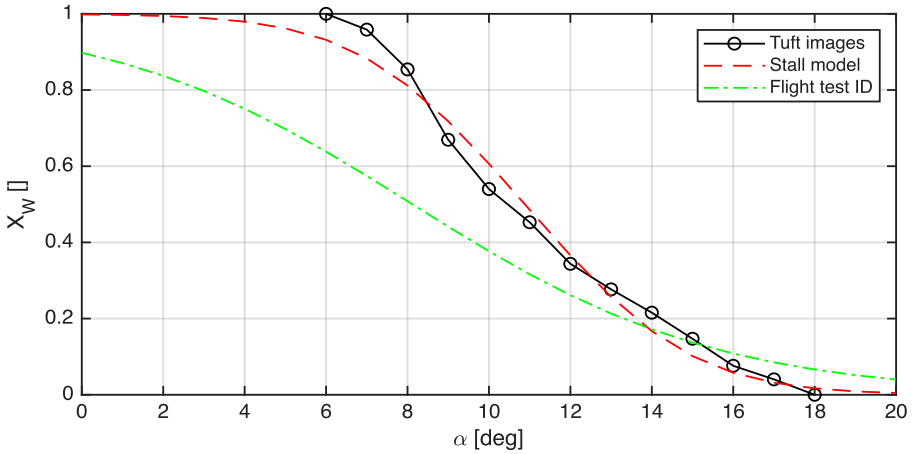


Figure 5: Stall model predictions for the GTT's main wing.

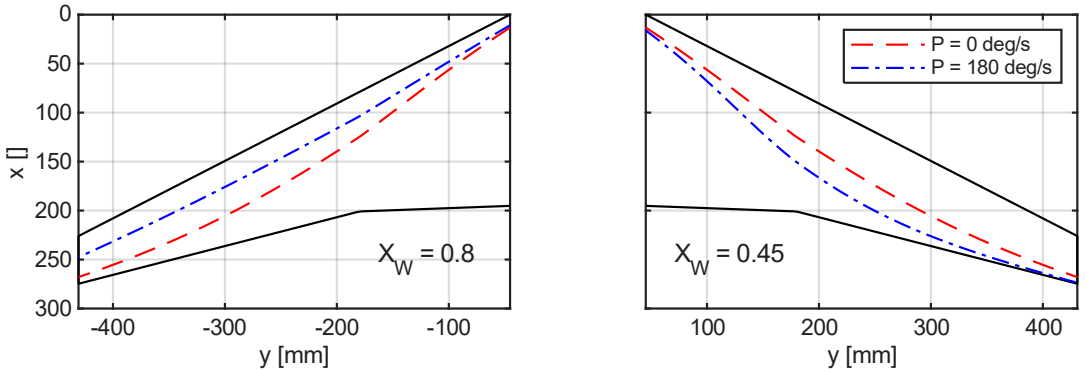


Figure 6: Predicted flow separation patterns from identified stall model at AoA = 10°.

To complete the stall model definition, equations (1)-(6) have to be expanded with additional terms that are a function of the wing stall parameter (Eq. (11)). A suitable model for lift and drag was already proposed in [6] and is re-used here, but with the new wing separation parameters $X_{W\,\text{left}}$ and $X_{W\,\text{right}}$ substituted accordingly:

$$C_{L\,\text{left/right}} = 0.5\left[(C_{L0} + C_{L\alpha}\,\alpha)\sqrt{X_{W\,\text{left/right}}} + C_L^*\,\sin(2\alpha)\,\sqrt{1 - X_{W\,\text{left/right}}}\right] \qquad (12)$$

$$C_L = C_{L\,\text{left}} + C_{L\,\text{right}} + C_{L\hat{Q}}\,\hat{Q} + C_{L\delta_S}\,\delta_{stab} \tag{13}$$

$$C_D = C_{D0} + \frac{C_L^2}{\pi\, e\, AR} + C_D^*\,\sin^2(\alpha)\left(1 - \frac{X_{W\,\text{left}} + X_{W\,\text{right}}}{2}\right) \tag{14}$$

For the pitching moment on the other hand, the equations identified in [6] must be fully retained. The reason for this is that the improved stall model presented here is incapable of capturing the complex downwash pattern behind the main wing and rear-mounted engine nacelles, both of which have been shown to severely influence the pitch behaviour. Nevertheless, the original model (Eq. (15)-(17)) already proved to be well suited to predicting pitch characteristics.

$$X_{W2} = 0.5\left[1 - \tanh\left(s_{W2}\,(\alpha - \alpha^*_{W2})\right)\right] \tag{15}$$

$$X_H = 0.5\left[1 - \tanh\left(s_H\,(\alpha - \alpha^*_H)\right)\right] \tag{16}$$

$$C_m = C_{m0} + C_{m\alpha}\,\alpha + C_{mX_W}\,(1 - X_{W2}) + C_{mX_H}(1 - X_H) + C_{m\hat{Q}}\,\hat{Q} + C_{m\delta_S}(0.25 + 0.75\,X_H)\,\delta_{stab} \tag{17}$$

The longitudinal aerodynamic forces and moments calculated with Eq. (12)-(17) are plotted in Figure 7. At low AoA and in the post-stall region, the model compares well with wind tunnel data but in the immediate stall region, where flight test results are in disagreement with wind tunnel predictions, clear differences exist. The justification that this is an improvement will be shown towards the end of this section.

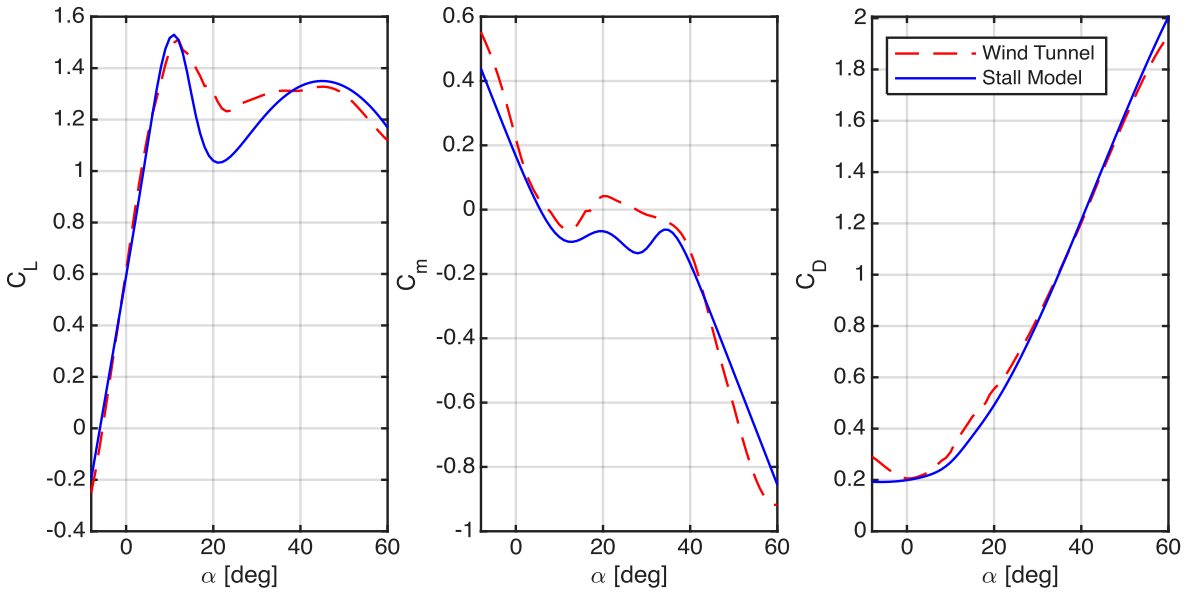


Figure 7: Longitudinal forces and moments from stall model.

The GTT stall model previously identified in [6] omitted lateral stall dynamics altogether, a shortcoming which is attempted to be overcome here. From wind tunnel experiments we know that the dominant lateral nonlinearities at stall are roll damping and aileron effectiveness. These may be approximated by two constants at low AoA ($C_{l\hat{p}0}$, $C_{l\delta_A 0}$) and a post stall reduction factor (k_l^*), with a smooth transition at stall (Eq. (18)-(19)).

$$C_{l\hat{p}} = C_{l\hat{p}0}\left(k_l^* + (1 - k_l^*)\sqrt{\frac{X_{W\,\text{left}} + X_{W\,\text{right}}}{2}}\right) \tag{18}$$

$$C_{l\delta_A\,\text{left/right}} = C_{l\delta_A 0}\left(k_l^* + (1 - k_l^*)\,X_{A\,\text{left/right}}\right) \tag{19}$$

The coefficients $C_{l\hat{p}0}$ and $C_{l\delta_A 0}$ can be directly taken from the linear model (Eq. (5)). The reduction factor k_l^* could be identified from flight test data, but insufficient suitable manoeuvres were flown during the GTT free-flight campaign to support this. Therefore, $k_l^* = 1/3$ is estimated here based on existing

GTT wind tunnel data. Equation (19) also introduces a new flow parameter $X_{A\,\text{left/right}}$, which is simply the area of attached flow within the spanwise aileron sections:

$$X_{\text{A left/right}} = \frac{\int_{y_{\text{ail root}}}^{y_{\text{ail tip}}} X_C\, c\, \text{dy}}{\int_{y_{\text{ail root}}}^{y_{\text{ail tip}}} c\, \text{dy}} \tag{20}$$

In addition to the roll damping loss modelled in Eq. (18), large rolling moments may also occur in the vicinity of stall due to asymmetric flow separation (Figure 3). These moments can be easily calculated from the individual components of lift on the left and right wing (Eq. (12)), assuming the forces act at the spanwise aerodynamic centre y_{MAC}. The total rolling moment is then computed as follows:

$$C_l = C_{l\hat{P}}\,\hat{P} + \left(C_{L\,\text{left}} + C_{L\,\text{right}}\right) y_{\text{MAC}} + C_{l\delta_A\,\text{left}}\,\delta_{\text{ail,left}} + C_{l\delta_A\,\text{right}}\,\delta_{\text{ail,right}} \tag{21}$$

This equation is evaluated at three representative roll rates and compared to wind tunnel data[4] in Figure 8. The stall model follows the reduction in roll damping with AoA very well, which is especially noteworthy since this is an implicit result of identifying stall progression from tuft data. Near stall, the model predicts a significantly larger destabilisation, which implies a greater tendency for the aircraft to exhibit wing rock.

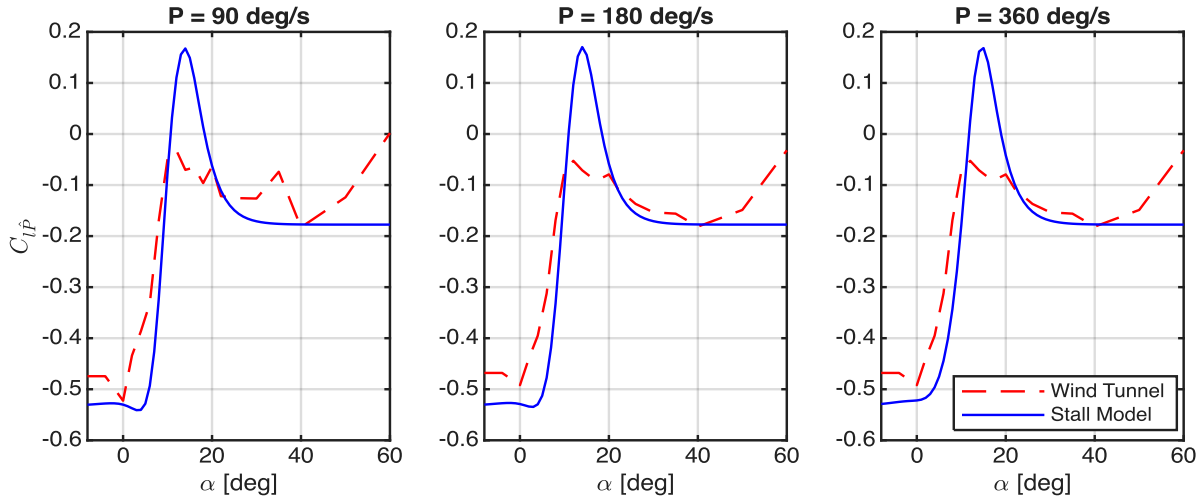


Figure 8: Lateral stall model compared to NASA wind tunnel data.

Similarly, aileron effectiveness is depicted in Figure 9. Once again, the early loss of control authority is purely defined by the flow separation over the aileron surfaces (Eq. (20)).

[4] NASA data is shown since dynamic derivatives were not measured during UoB wind tunnel tests.

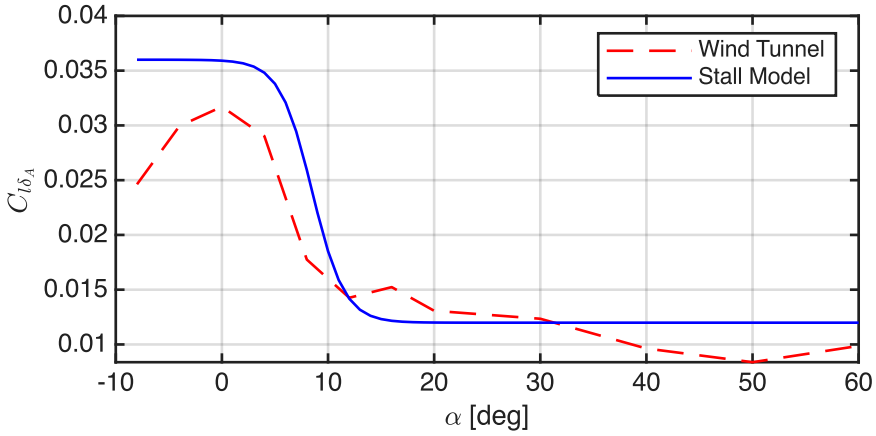


Figure 9: Aileron control effectiveness for the stall model compared to wind tunnel data.

Directional aerodynamics were not the principal subject of this work since yaw stability is mostly decoupled from the wing stall discussed here and is additionally influenced by vertical tail lift, flow blockage from the fuselage and engines, and fuselage forebody crossflow [6]. Nevertheless, a simple directional stall model based on the methodology outlined so far for the main wing is proposed:

$$X_V = 0.5\left[1 - \tanh\left(s_V\left(\alpha_0 - \alpha_V^*\right)\right)\right] \tag{22}$$

$$C_n = \left(C_{n\beta\,0}\, X_V + C_{n\beta}^*\left(1 - X_V\right)\right)\beta + C_{n\hat{P}}\,\hat{P} + C_{n\hat{R}}\,\hat{R} + C_{n\delta_A}\left(\delta_{ail,\text{left}} + \delta_{ail,\text{right}}\right) + C_{n\delta_R\,0}\sqrt{X_V}\,\delta_{rud} \tag{23}$$

All parameters are exclusively identified from wind tunnel data. Figure 10 shows how the static and dynamic stability derivatives, as well as the rudder control effectiveness, vary with AoA. Despite the lack of flight test corrected data here, it is expected this has a small effect on wing rock since good directional stability is maintained up to a larger AoA than in the lateral axis.

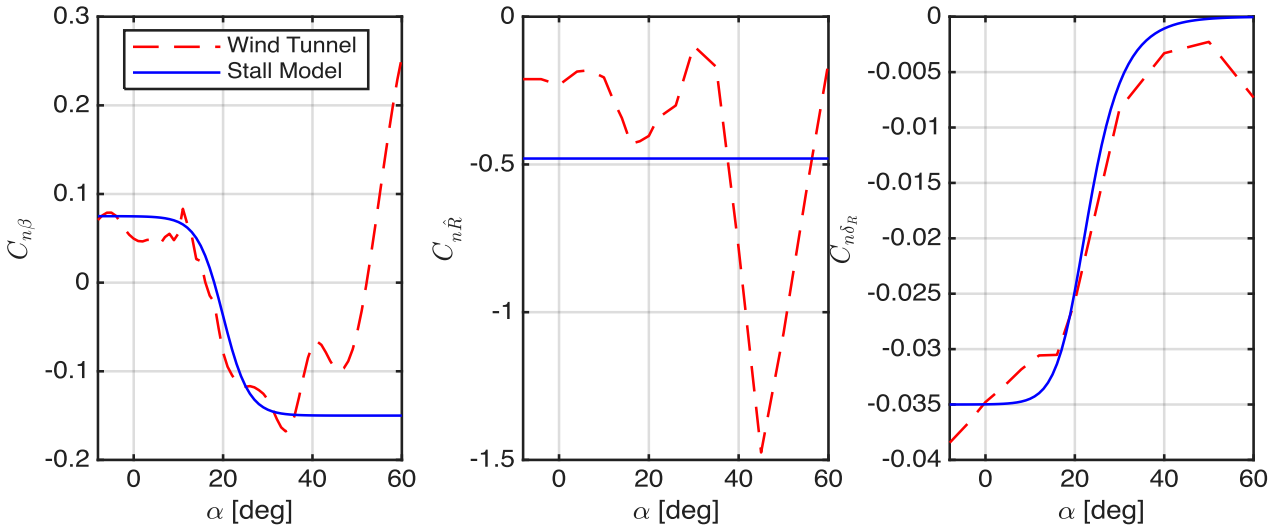


Figure 10: Directional aerodynamics of the stall model compared to wind tunnel data.

To validate the stall model against flight test data, nonlinear 6-DOF time series simulations were conducted. Both the new stall model and the numeric wind tunnel model were used to reproduce flight test results. These simulations are initialised from the flight test conditions at the beginning of the clipped manoeuvre and commanded control surface positions are prescribed as inputs. Two such simulations are shown here.

Figure 11 depicts a longitudinal approach to stall, where wings were kept approximately level by a closed-loop bank angle controller. The aircraft was flown close to stall with the assistance of a pitch

command augmentation system and large AoA oscillations were encountered. The simulation trace based on wind tunnel data passes the unstable pitch break and settles at a post-stall trim condition for a while until recovery inputs are applied. This is clearly in disagreement with the observed flight test result and hints at inaccurate pitching moments near stall in the wind tunnel data. The presented stall model on the other hand reveals a different pitch-up characteristic (Figure 7) that closely matches the flight test in the time series simulation.

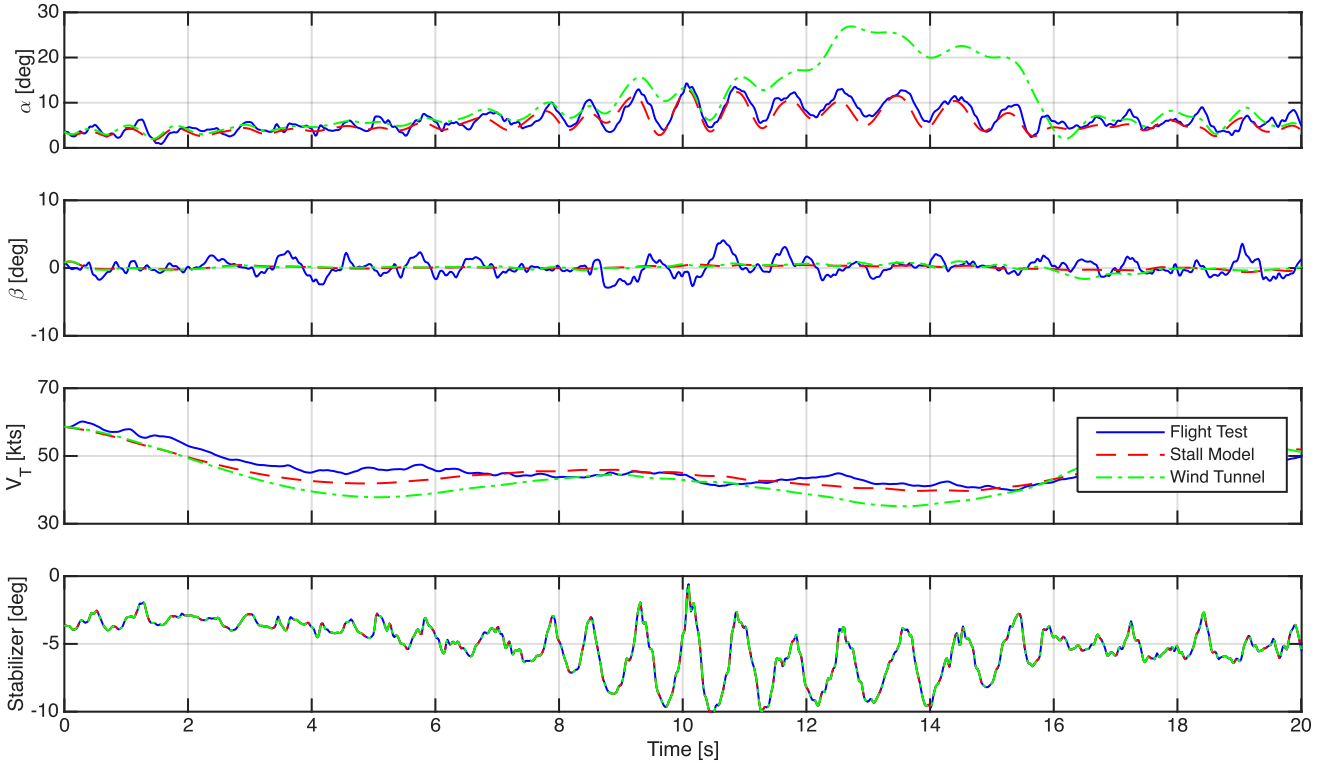


Figure 11: Longitudinal stall: flight test compared to stall model and wind tunnel predictions,

Figure 12 shows a fully open-loop stall test, meaning that all controls except for the stabiliser were zeroed and the pure motion of the aircraft was observed. In this case, a wing rock develops well before stall is reached but neither the stall model nor the wind tunnel data predicts this correctly, despite clearly capturing the significant degradation of lateral stability (Figure 8). This issue was already discussed in [6] and is attributed to the fact that flight tests are always subject to external disturbances such as winds, turbulence, and small unintentional built-in asymmetries in the aircraft and its control system. Since the GTT's Dutch roll mode becomes unstable as AoA increases during an approach to stall, small disturbances can quickly grow into large oscillations. Disturbances can be introduced in the simulations and indeed trigger a wing rock, although the result will inevitably depend on the type and amplitude of the disturbance introduced, which makes this technique unsuitable for predicting wing rock characteristics.

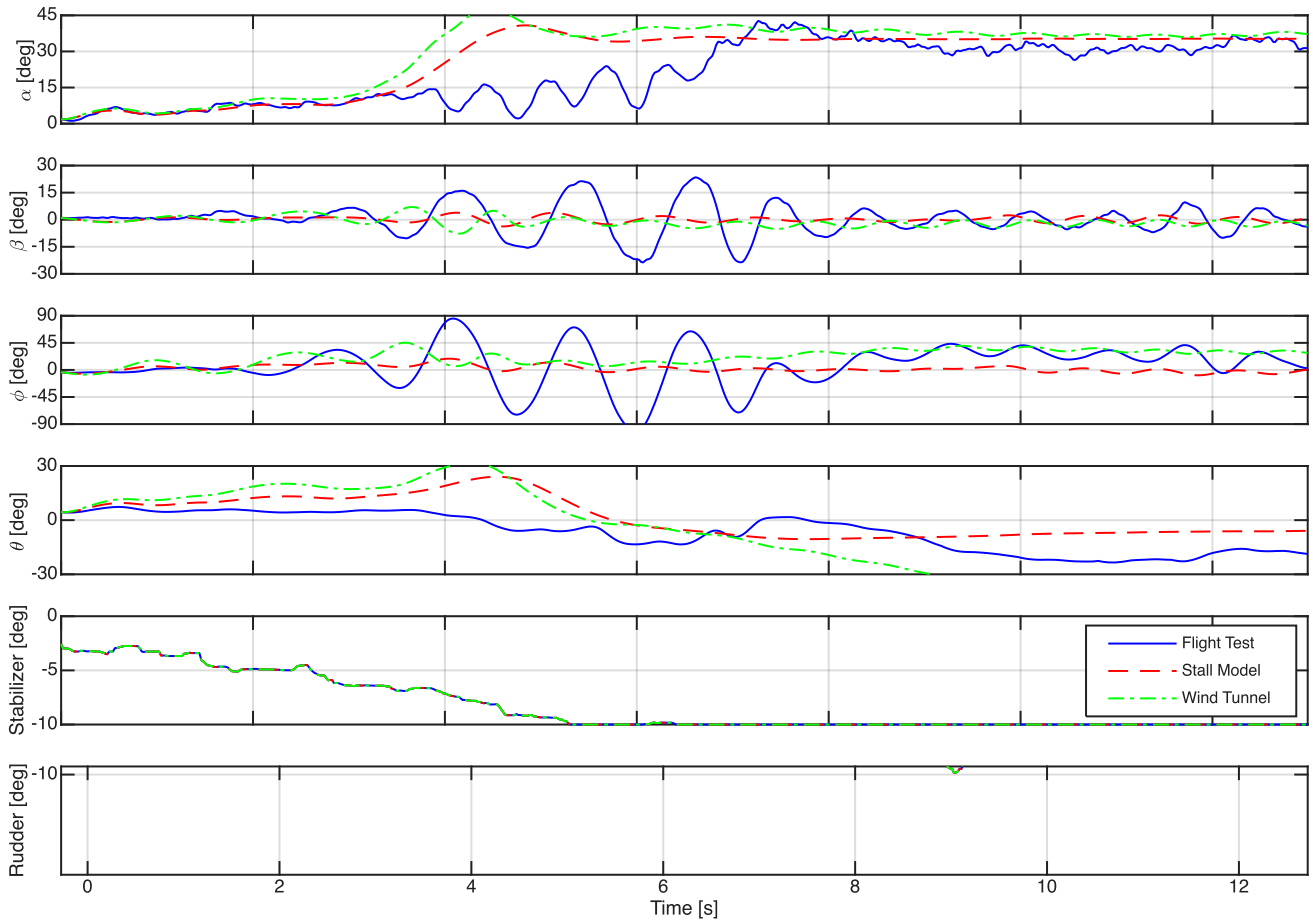


Figure 12: Stall test with wing rock: flight test compared to stall model and wind tunnel predictions.

4. Results

As described above, the flight test traces reveal nonlinear phenomena at angles of attack approaching stall, in particular pitch-up and a limit cycle oscillation which is dominant in roll. These are also captured in the numerical flight mechanics model with the aerodynamics represented as outlined above, and can be observed in time history simulations (with a lateral-directional perturbation required to reveal the wing rock).

Alternatively, the mechanisms underlying these phenomena can be observed via the steady state solutions and their stability as presented in a bifurcation diagram. A bifurcation diagram indicates all branches of stable and unstable equilibria and periodic orbits (limit cycles) over a range of, typically, one varying parameter – known as the continuation parameter (CP); other forms of diagram can be generated but in this paper only one-parameter bifurcation diagrams are shown. Note that a feature of nonlinear systems is the potential existence of multiple steady state solutions for a given set of parameter values.

The steady state solution branches serve as the ‘structure’ that prescribes the qualitative nature of the system behaviour; specific responses involving transient dynamics will depend on the inputs and initial conditions but will always be governed by the underlying steady state structure. Bifurcation diagrams have been used previously to gain insight into the mechanisms governing airliner nonlinear flight dynamics (e.g. [8]).

In the diagrams to be shown here, line colours and markers are defined as follows:

blue solid line	stable equilibrium solutions
red dashed lines	unstable equilibrium solutions
orange solid line	stable limit cycle solutions (min. and max. amplitudes)
orange dashed line	unstable limit cycle solutions (min. and max. amplitudes)
*	Hopf bifurcation points, where a branch of equilibrium solutions changes stability and a limit cycle oscillation is born or terminates (depending on the direction of change of the parameter that is being varied).

The CP is always stabiliser deflection, δ_{stab}, with aileron, elevator and rudder set to zero – replicating the conditions under which the stall/deep stall flight tests were conducted. The stabiliser deflection range of the GTT is $-10°$ (trailing edge up) to $+5°$ (trailing edge down). The CG position is at 21% of mean aerodynamic chord (mac) unless stated otherwise, again matching the flight test condition.

Figure 13 shows the AoA (α), sideslip (β), roll rate (p) and bank angle (ϕ) bifurcation diagram projections generated from the flight mechanics equations with the stall model. Diagrams for the remaining four states (flight velocity, pitch rate, yaw rate and pitch angle) are not shown, in the interests of brevity.

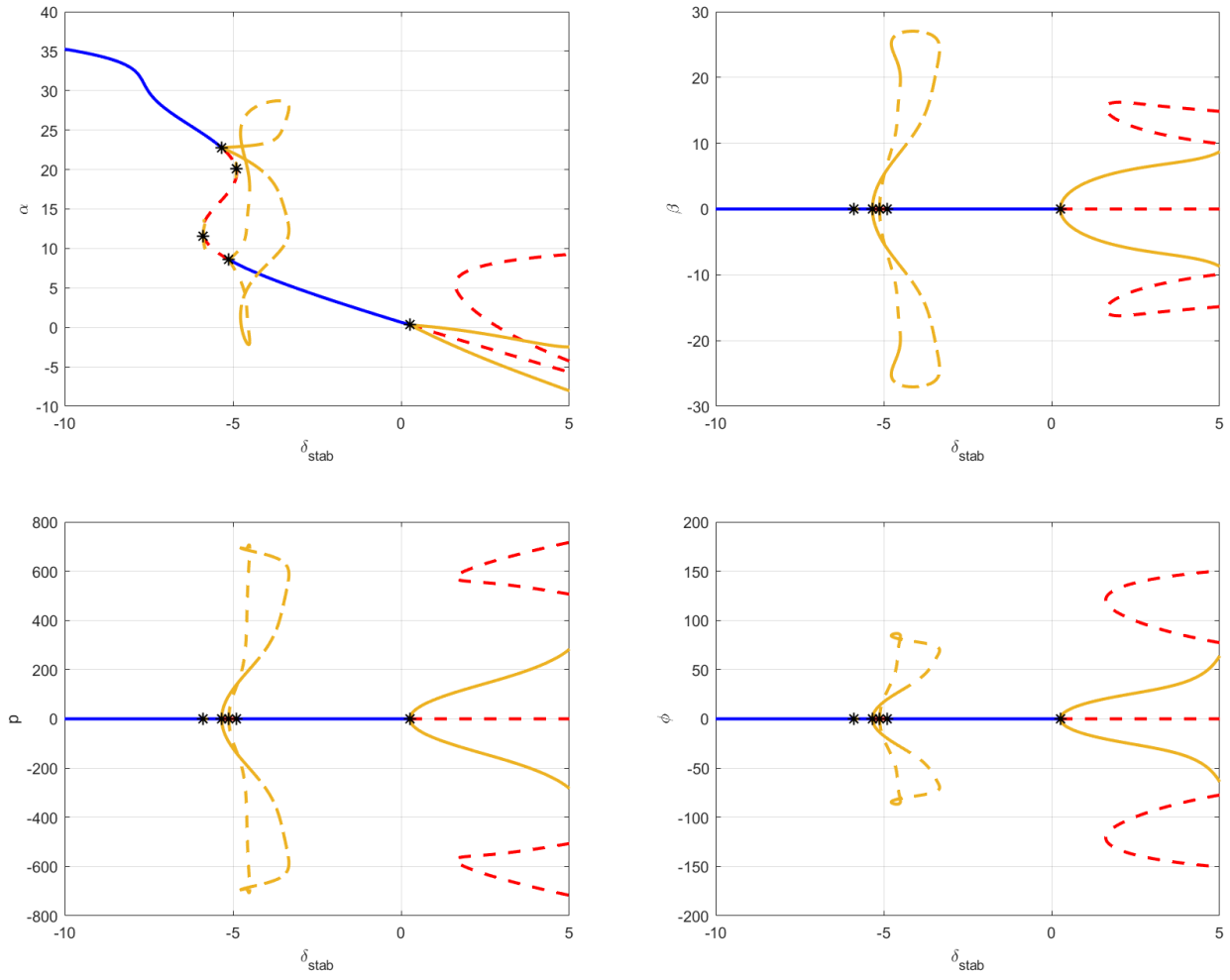


Figure 13: Numerical bifurcation diagram projections in α, β, p and ϕ (all units in degree).

There is a branch of equilibrium solutions for which all lateral-directional variables are zero, reflecting the symmetry of the model in terms of aerodynamics, geometry and mass distribution. At negative angles of attack, corresponding to positive δ_{stab} values, the equilibria are unstable and a stable limit cycle exists; the oscillations are quite large in all state variables other than speed and pitch angle and

all lateral-deflection quantities oscillate symmetrically with respect to zero (i.e. with equal magnitude both 'left' and 'right'); amplitude increases as δ_{stab} increases. This branch is attributed to the lightly-damped Dutch roll mode, which becomes unstable at negative AoA. Therefore, the unstable, but symmetric, branch represents the longitudinally-stable trim conditions, whereas the stable limit cycles map the ensuing Dutch roll eigenmode that develops for any lateral disturbance. There is also a pair of unstable equilibrium solutions at excessively high roll rates, representing an autorotation condition.

However, the aerodynamic model and associated experimental campaign focus on the positive angles of attack and in particular the stall region. Between zero and 8.59° AoA the equilibria are stable, as expected in an airliner's normal flight regime. At $\delta_{stab} = -5.12°$ and $\alpha = 8.59°$ the equilibria lose stability via a Hopf bifurcation to a limit cycle whose minima and maxima have a complicated-looking shape with two folds such that some parts of the oscillation are stable and others unstable. It rejoins the equilibrium branch again at another Hopf point at $\delta_{stab} = -5.33°$ and $\alpha = 22.8°$. The eigenvalues of the linearised system on the equilibrium branch show that the change of stability at the Hopf points is associated with the Dutch roll mode, as previously mentioned. Figure 13 shows the limit cycle that arises at these points is dominant in roll and can be classified as wing rock.

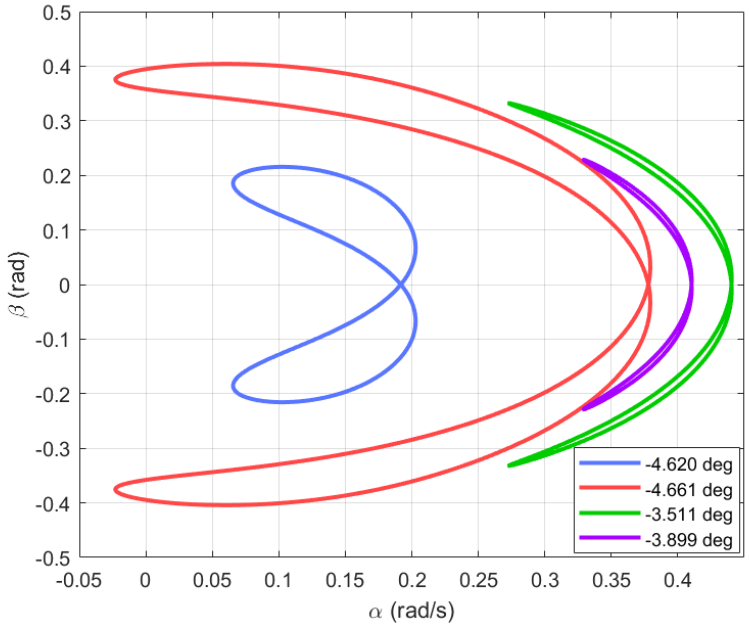


Figure 14: Limit cycle phase plane plots in α and β at four different stabiliser values.

Figure 14 shows phase plane plots of the wing rock limit cycle at four different δ_{stab} values. In three of the cases ($-4.661°$, $-3.511°$ and $-3.899°$) the limit cycle exhibits clear kinematic coupling: an exchange of α and β as the aircraft rolls, with a 90° phase shift between them. The other case ($\delta_{stab} = -4.62°$) is close to the Hopf bifurcation point at $\alpha = 22.8°$.

There are two other Hopf bifurcation points between the two already referred to. The oscillations arising from these are purely longitudinal and of very small amplitude: they can be ignored here in terms of the observable behaviour of the aircraft.

The symmetric equilibrium branch regains stability for AoA higher than $22.8°$. Thus the aircraft model exhibits stable symmetric post-stall behaviour to very high incidence. The α bifurcation diagram reveals that this is recoverable by simply increasing δ_{stab} so it is not considered to be deep stall (which is typically unrecoverable in this way). Note that if the CG is moved aft, the numerical model symmetric equilibria branch 'stretches' across a wider range of δ_{stab} so that the stable high AoA equilibria exists across the entire available physical range of stabiliser – signifying deep stall. This is shown in the α and ϕ bifurcation diagram projections for CG at 40%mac in Figure 15.

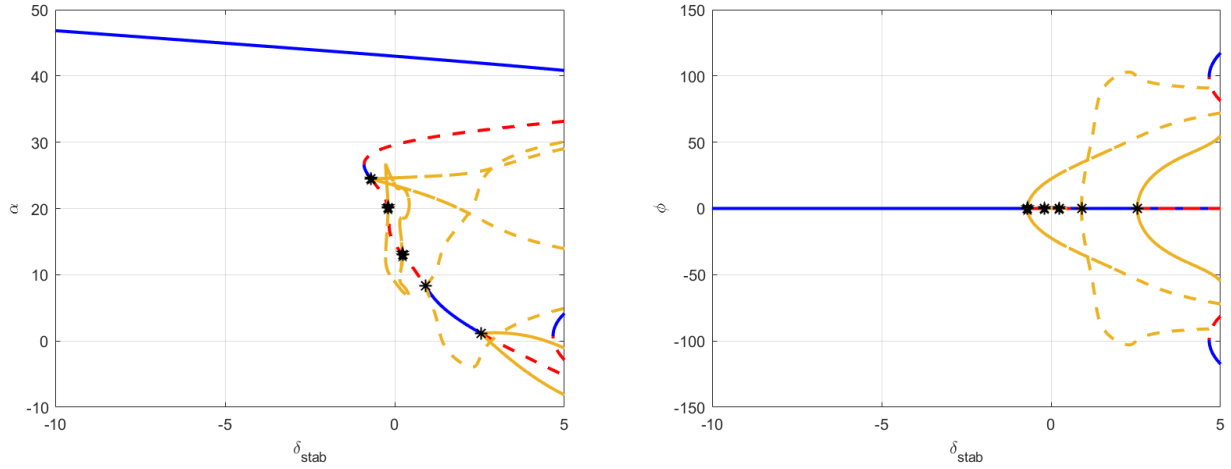


Figure 15: Numerical bifurcation diagram projections in α and ϕ, CG=40%mac (all units in degree).

We now return to the case of CG at 21%mac in order to compare predicted behaviour from the numerical model with a flight trace in which the aircraft was flown through the stall into the post-stall region. **Error! Reference source not found.** shows the same α and β bifurcation diagrams as in Figure 13 with the flight test trace superimposed (asterisk line type). If the numerical model faithfully captured the aircraft's behaviours, it would be expected that for a very slow (quasi-steady) variation of the continuation parameter, δ_{stab}, the flight test trace would match the bifurcation diagram: as the stick is pulled back (more negative δ_{stab}), the α and β would both oscillate between their respective minimum and the maximum limit cycle amplitude values indicated in the bifurcation diagram, and then converge onto the stable equilibria for $\alpha > 22.8°$.

However, in the flight test the stabiliser incidence was increased continuously at a rate of approximately 1.5°/s, causing a transient response rather than a steady state. This, together with the pitch instability at stall, brought the aircraft rapidly through the wing rock region such that the oscillation does not develop within the expected δ_{stab} range. However, there is evidence of it developing and then the response is quickly attracted to the high AoA stable equilibrium $\alpha \approx 35°$ at $\delta_{stab} = -10°$ although the nature of the response converging on this condition can't be observed in this figure as it occurs over a time interval with δ_{stab} fixed at $-10°$.

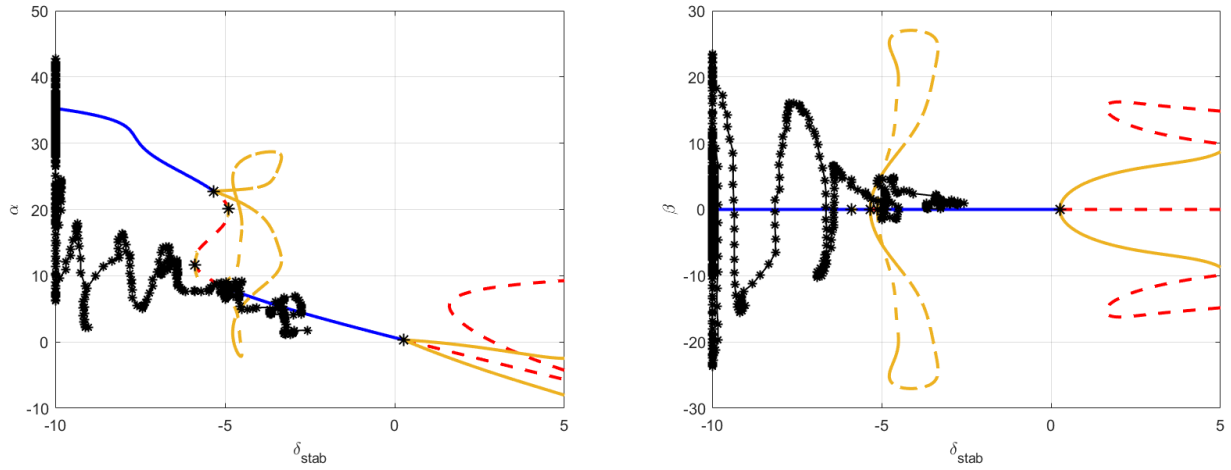


Figure 16: Flight test trace superimposed onto α and β bifurcation diagrams (all units in degree).

In order to better compare the flight test response with that of the numerical model (via the bifurcation diagram information), the test trace is now plotted against α rather than δ_{stab}. This is shown for both β and ϕ with limit cycle minimum and maximum bounds from the bifurcation analysis in Figure 17.

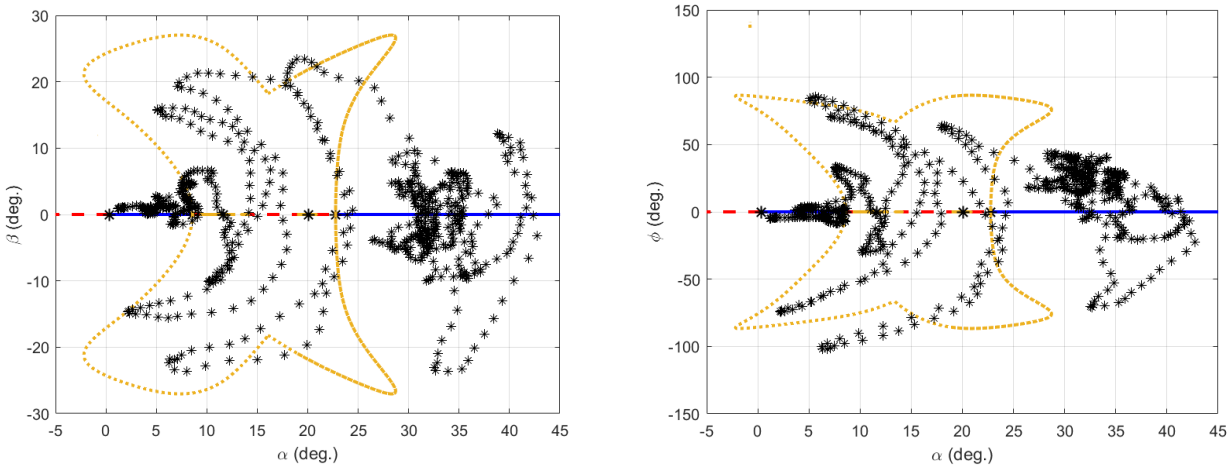


Figure 17: Flight test trace for β and ϕ against α, showing limit cycle maxima and minima boundaries from bifurcation analysis (all units in degree).

It is evident that the flight test traces conform to the limit cycle maxima and minima quite well, especially considering the 'extreme' nature of this flight phase in real-world atmospheric conditions and the extent of transient behaviour (as revealed in the convergence onto the high AoA equilibria). It is clearly seen that during flight test, the wing rock oscillations start at exactly the same AoA as predicted by the first bifurcation point. While the recorded test response represents a transient behaviour through the associated limit cycle branch, there is still enough data to show that the wing rock developed its maximum amplitude for at least two full cycles (refer to the time trace in Figure 12). The peak bank angles reached during the flight test match the bifurcation predictions very well. This stands out against the time simulations, which were not able to predict the severity of the wing rock accurately.

Transitioning into the high-AoA region, the limit cycle solutions collapse again into another stable branch. This is not representative of the recorded test data, which reveals a transition to a different oscillatory post-stall mode with smaller amplitudes. This is not surprising since the focus of the presented stall model lies in the immediate stall region and several aerodynamic effects at these extreme AoA were not incorporated due to their complexity. For this post-stall region, good results were previously achieved by applying the bifurcation method to the UoB wind tunnel data [7].

5. Conclusions

A stall model for swept-wing transport aircraft was presented. This model was identified from flight test recordings and wind tunnel flow visualisation, but its simple formulation allows the use of other data sources to determine the required parameters. For example, the model may use wind tunnel data during the design phase of an aircraft to make predictions about dynamic stability at stall, and later use flight test results to improve its accuracy. Another clear advantage over tabulated data is that the presented model is smooth and computationally efficient, therefore lending itself to advanced analysis methods such as the bifurcation analysis that was applied in this work.

The proposed stall model proved to be very effective in predicting the onset of wing rock, as well as the expected amplitude, when used in combination with numerical bifurcation analysis. The presented bifurcation diagrams intuitively depict wing rock dynamics and are more robust in terms of representing the parameter-dependence of the system dynamics than time series simulations. Longitudinal dynamics also match well to flight test results but are still based on a semi-empirical model developed in earlier work. Future improvements would need to look at the effects of the lift distribution on the wing's centre of pressure and the downwash interactions with the horizontal tail.

Ideally, the model definition and its use in generating bifurcation diagrams would have been carried out in parallel with the flight testing. Generally, when trying to understand complex nonlinear behaviours the numerical bifurcation analysis, accompanied by relevant time histories where appropriate, can

inform how to conduct the experiment; the latter then usually produces an opportunity to improve the numerical model and so the two aspects are iterated in order to refine the model and to obtain the experimental data needed. In this case, for example, slow quasi-steady stabiliser inputs would have helped to match the data to the bifurcation diagrams. However, it is not always the case that simple one-parameter variations can be achieved in flight where there are nonlinear phenomena and additional atmospheric inputs, and it may be necessary to deploy judicious application of feedback control to obtain the desired data.

6. Acknowledgements

The authors are grateful to the NASA Langley Research Center, specifically Kevin Cunningham and Gautam Shah, for providing the GTT model data and advice on its implementation.

7. Contact Author Email Address

mailto: m.lowenberg@bristol.ac.uk

8. Copyright Statement

© University of Bristol, 2026.

The authors confirm that their organization holds copyright on all of the original material included in this paper. The authors also confirm that they have obtained permission, from the copyright holder of any third party material included in this paper, to publish it as part of their paper. The authors confirm that they give permission, or have obtained permission from the copyright holder of this paper, for the publication and distribution of this paper as part of the ICAS proceedings or as individual off-prints from the proceedings.

References

[1] Cunningham, K., Shah, G., Hill, M., Pickering, B., Litt, J., & Norin, S. “A Generic T-tail Transport Airplane Simulation for High-Angle-of-Attack Dynamics Modeling Investigations”, AIAA Modeling and Simulation Technologies Conference, AIAA 2018-1168, 2018.

[2] Cunningham, K., Shah, G., Frink, N., McMillin, S., Murphy, P., Brown, F., Hayes, P., Shweyk, K. & Nayani, S. “Preliminary Test Results for Stability and Control Characteristics of a Generic T-tail Transport Airplane at High Angle of Attack”, 2018 AIAA Atmospheric Flight Mechanics Conference, AIAA 2018-0529, 2018.

[3] Cunningham, K., Shah, Murphy, P., G., Hill, M. & Pickering, B. “Pilot Sensitivity to Simulator Flight Dynamics Model Formulation for Stall Training”, 2019 AIAA Scitech Forum, AIAA 2019-0717, 2019.

[4] Pusztai, D, Lowenberg, M. & Simon A. Neild, S. “Static Wind Tunnel Testing of a Generic T-Tail Transport Airplane at High Angle of Attack”, 2023 AIAA SciTech Forum, AIAA 2023-0217, 2023.

[5] Pusztai, D, Lowenberg, M. & Simon A. Neild, S. “Flight Testing of a Dynamically Scaled Transport Aircraft Model for High-Alpha Wind Tunnel Data Validation”, 2024 AIAA SciTech Forum, AIAA 2023-1497, 2024.

[6] Pusztai, D. “Upset Dynamics and Deep Stall of the NASA Generic T-Tail Transport Aircraft”, PhD thesis, University of Bristol, UK, Dec. 2024.

[7] Pusztai, D, Lowenberg, M. & Simon A. Neild, S. “Computational and experimental study of deep stall in a generic T-Tail transport aircraft”, 2025 AIAA SciTech Forum, AIAA 2025-1054, 2025.

[8] Gill, S., Lowenberg, M., Neild, S., Krauskopf, B., Puyou, G., and Coetzee, E. “Upset dynamics of an airliner model: A nonlinear bifurcation analysis,” Journal of Aircraft, Vol. 50, no. 6, Dec. 2013, pp. 1832–1842.

[9] Fischenberg, D. “Identification of an unsteady aerodynamic stall model from flight test data,” AIAA 95-3438-CP, 20th Atmospheric Flight Mechanics Conference, Baltimore, MD, August 1995. https://doi.org/10.2514/6.1995-3438.

[10] Jategaonkar, R. V., Fischenberg, D., Gruenhagen, W. “Aerodynamic Modeling and System Identification from Flight Data—Recent Applications at DLR,” AIAA Journal of Aircraft, Vol. 41, No. 4, 2004, pp. 681-691. https://doi.org/10.2514/1.3165.

[11] Herbold, J. A., Pool, D. M., de Visser, C. C. “Improved Longitudinal Stall Modeling with Separable Nonlinear Least Squares and Dynamic Stall Maneuvers,” Proceedings of the 2026 CEAS EuroGNC conference, Madrid, Spain, May 2026.